

Publication III

J. Salo, J. Meltaus, E. Nojonen, M. M. Salomaa, A. Lönnqvist, T. Koskinen, V. Viikari, J. Säily, J. Häkli, J. Ala-Laurinaho, J. Mallat, and A. V. Räsänen, “Holograms for shaping radio-wave fields,” *Journal of Optics A: Pure and Applied Optics*, vol. 4, no. 5, pp. S161–S167, Sep. 2002.

© 2002 IOP Publishing Limited. Reprinted with permission.

Journal homepage at <http://www.iop.org/journals/jopa>

This article at <http://www.iop.org/EJ/abstract/1464-4258/4/5/365>

Holograms for shaping radio-wave fields

Janne Salo¹, Johanna Meltaus¹, Eero Noponen^{1,2},
Martti M Salomaa¹, Anne Lönnqvist², Tomi Koskinen²,
Ville Viikari², Jussi Säily², Janne Häkli², Juha Ala-Laurinaho²,
Juha Mallat² and Antti V Räisänen^{2,3}

¹ Materials Physics Laboratory, Helsinki University of Technology, PO Box 2200,
FIN-02015 HUT, Finland

² MilliLab, Radio Laboratory, Helsinki University of Technology, PO Box 3000,
FIN-02015 HUT, Finland

E-mail: Janne.Salo@hut.fi

Received 10 December 2001, in final form 7 March 2002

Published 14 August 2002

Online at stacks.iop.org/JOptA/4/S161

Abstract

Holograms—diffractive elements—are designed and fabricated for shaping millimetre-wave radio fields. Methods for the synthesis of hologram elements are discussed and several beam shapes are tested: plane waves, radio-wave vortices and Bessel beams. Here we present an overview of the methods applied and results obtained with quasi-optical hologram techniques using both amplitude and phase holograms.

Keywords: Millimetre-wave technology, holographic gratings, Bessel beams, radio-wave vortices

(Some figures in this article are in colour only in the electronic version)

1. Introduction

Computer-generated holograms [1, 2] have found a wide range of applications within and near the visible range of the electromagnetic spectrum [3]. Here we consider radio holograms in the millimetre- and submillimetre-wave regimes, whose primary application has thus far been in the compact antenna test range (CATR) at 119 GHz [4]. The CATR based on an amplitude hologram has also been demonstrated at submillimetre-wavelengths with a 60 cm hologram for 310 GHz [5], and one of the principal objectives is the development of a hologram for 650 GHz.

We have also investigated the generation and the properties of novel beam shapes using the radio-waves, together with possible new applications of both amplitude and phase holograms at millimetre- and submillimetre-wavelengths. Radio holograms may be utilized to generate radio-frequency beams that are better known in optics, such as nondiffracting Bessel beams [6–8] (also produced with a radio-frequency axicon [9]) and electromagnetic vortices that are analogues to the so-called optical vortices [10].

³ Presently visiting: Observatoire de Paris, 61 Avenue de l'Observatoire, 75014 Paris, France.

This paper is organized as follows. Section 2 discusses the amplitude- and phase-hologram techniques. The design methods employed are described in section 3. Section 4 outlines the experimental set-up used to record the generated radio-wave beam forms. Experimental results for plane waves, radio-field vortices and Bessel beams generated with the help of amplitude holograms are reported in section 5. Here we also present preliminary results for a beamsplitter generated with a phase-type hologram.

2. Hologram techniques

Computer-generated holograms are locally periodic diffraction gratings that modify both the reflected and transmitted electromagnetic fields. In all the hologram techniques considered in this paper, the transmitted field is optimized for the desired output while the reflected field is ignored.

Radio holograms are computer-generated holograms that operate with monochromatic radio waves. They are usually designed to perform a simple holographic function with high quality, such as forming a propagating plane wave from an incident Gaussian beam. Similarly, other beam forms, including radio-wave vortices and Bessel beams, can be formed by using appropriately fabricated radio holograms.

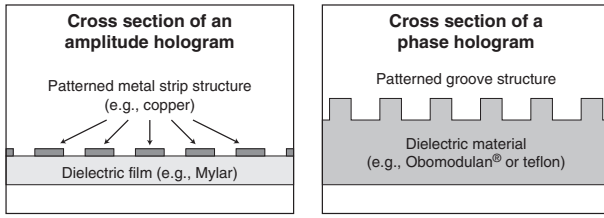


Figure 1. Local grating structure of amplitude (lhs) and phase holograms (rhs).

2.1. Amplitude holograms

In the amplitude-type radio holograms used in this work, the diffraction grating consists of metallic (copper) stripes on a dielectric film. We have used a Mylar film (75 μm thick, relative permittivity $\epsilon_r = 3.3$) with a copper layer (17 μm) on top, see figure 1. In the millimetre-wave region, the skin depth of the radio field within the copper is far less than 1 μm ; hence the metallic grating effectively reflects all the radio-frequency field incident on the copper stripe and transmits the field through the slots between the stripes. Consequently, the transmitted field is effectively modulated with a binary function corresponding to the hologram grating. The transmitted field is then diffracted according to the wavelength-scale structure caused by the hologram.

Figure 2 shows an example of a binary amplitude hologram used to produce the zeroth-order Bessel beam $E = J_0(\alpha r)e^{i\beta z}$ (with α and β being constants that satisfy $\alpha^2 + \beta^2 = k^2$, where $k = 2\pi/\lambda$ is the wavenumber) [6, 11]. The phase is modulated by the locations of the slots and the amplitude is modulated by the variations of the slot widths. The hologram is designed to transmit the beam at an angle $\theta = 33^\circ$. The slots are narrowed (tapered) on the edge of the hologram pattern; this reduces unwanted edge diffractions.

2.2. Phase holograms

In phase-type holograms, the hologram structure features locally changing effective thickness seen by the electromagnetic wave; this can be realized by varying either the index of refraction or the depth of the surface profile. In our work, the hologram elements consist of milled grooves on a dielectric substrate, see figure 1. The material used is Obomodulan[®], which is suitable for high-finesse milling and has $\epsilon_r \approx 2.2$. The field passing through the grooves acquires a phase difference with respect to that between the grooves, leading to a phase modulation of the transmitted field, instead of amplitude modulation.

Phase-type elements generally provide a higher efficiency than their amplitude counterparts since their operation is not based on the partial blocking of the incident field. There are, however, always some losses due both to the reflection of the radio field on the interface of a dielectric material and due to the attenuation within a lossy dielectric. The groove profile of phase holograms may be binary (all grooves have rectangular cross sections), multilevel (stepped profile) or continuous; rigorous electromagnetic modelling is needed to optimize the grating structure [12].

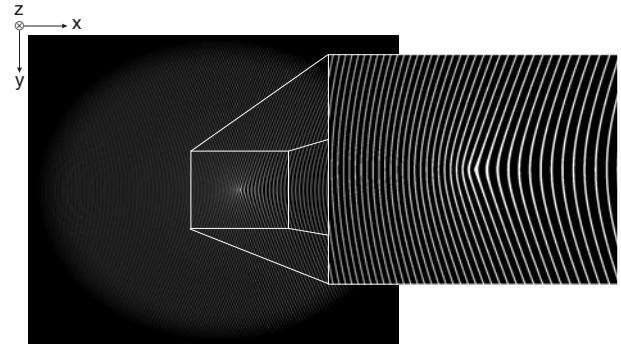


Figure 2. The binary amplitude hologram pattern used to produce the zeroth-order Bessel beam. The pattern is tapered in order to limit the aperture and to reduce edge diffractions. Nontransparent stripes are indicated in black and the transparent slots in white.

3. The design and synthesis of holograms

The physical operation of a (thin) holographic grating is described with a transmission function, i.e. the transmittance $T(x, y)$ that relates the transmitted electromagnetic field to the incident field according to $E_{tr}(x, y) = T(x, y)E_{in}(x, y)$. For nonamplifying hologram substrates, $T(x, y)$ is a complex function with $|T| \leq 1$. There exist several schemes for designing grating structures that should approximately yield the desired transmittance, see, for instance, [1–3]. For amplitude holograms, as discussed in section 2.1, this often leads to a binarized transmittance $T_b(x, y)$ consisting of transparent ($T_b = 1$) and opaque ($T_b = 0$) regions.

3.1. Electromagnetic modelling

The binarized transmission function $T_b(x, y)$ determines the structure of the hologram (i.e. it selects the areas where the metal is etched off). Nevertheless, the function is insufficient to describe the actual transmission through the narrow slots of the hologram. In practice, the transmission depends on the polarization of the incident field and the widths of the slots. In addition, the effect of the dielectric substrate film cannot be excluded.

Here the electromagnetic modelling and analysis is based on the finite-difference time-domain (FDTD) method, see [13], followed by the use of physical optics. Due to the enormous size of the hologram and the numerous small-scale details (i.e. slots and stripes) the direct electromagnetic analysis of an entire hologram would require massive computing effort, even for supercomputers. Therefore, the electromagnetic problem has to be simplified and reduced. The fair agreement between the simulation and measurement results has indicated that the electromagnetic modelling based on the two-dimensional FDTD method is applicable. In the two-dimensional method, the hologram structure is assumed to be infinite and invariant in the y direction, see figure 3. In studying the electromagnetic behaviour in the narrow x -directed area, this is a fair approximation due to the gentle curvature of the slots and the stripes in the y direction. Binary amplitude holograms of this type are used in the CATR applications; for their design methods, see [14]. Apparently, this modelling method would also be appropriate for phase holograms with a similar geometry.

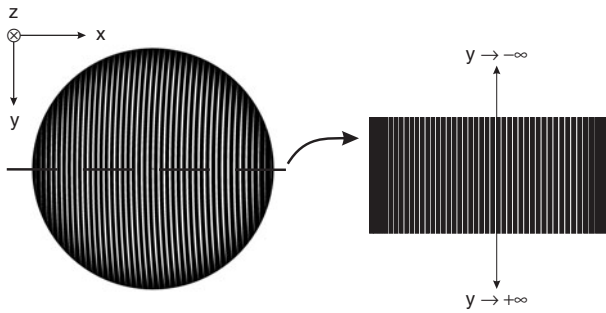


Figure 3. Simplification of a CATR hologram used in the FDTD simulation.

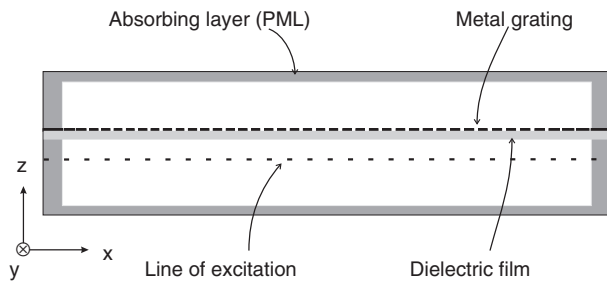


Figure 4. Two-dimensional FDTD simulation domain.

A scheme of the two-dimensional FDTD simulation is shown in figure 4. The simulation domain is divided into cells: within each cell, local and time-dependent electric and magnetic fields are computed with Maxwell's equations using the central-difference approximation. In the two-dimensional FDTD simulation, two different polarizations are studied separately; the electric field is either parallel with the slots (y -directed) or perpendicular to them (tangential to the (x, z) -plane). The magnetic field is perpendicular to the electric field. So far, holograms are always designed with the electric field parallel with the slots, i.e. the electric field of the feed horn is vertically polarized. In the two-dimensional simulations the curvature of the slots, and at the same time the source of the cross polarization, are omitted; the cross polarizations produced by holograms in the CATR application are studied in [15].

The simulation domain is very wide in the x direction (up to tens of thousands of FDTD cells) but quite narrow along the z axis (a couple of dozen cells). At the line of excitation, the complex feed horn field is added to the electric field, see figure 4. The simulation domain is surrounded with an absorbing layer that serves to simulate the radiating free-space condition. We have used the so-called perfectly matched layer (PML) which has a very low reflection coefficient [16].

As a result of the FDTD simulation, the field in the hologram aperture is obtained. The transmitted field away from the hologram is calculated with physical optics on the same (x, z) -plane where the aperture field is simulated. It is optimized first on the plane $y = 0$ (i.e. along the centre-line of the hologram, see figure 3) and then the field quality is verified on the other planes. If necessary, the hologram pattern can be locally modified in the y direction.

Figure 5 shows the full simulated radiation pattern of a 1 m diameter hologram operating at 650 GHz. The pattern is

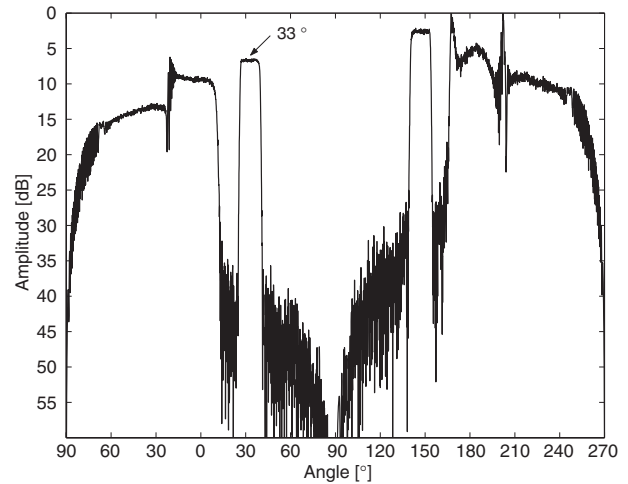


Figure 5. Full simulated horizontal radiation pattern of a 650 GHz hologram. Here, 0° is the hologram normal. The hologram is designed to form a plane wave that propagates at the angle of 33° . The reflected amplitude pattern is seen in the angular range from 90° to 270° . The flat peak at 147° is due to backscattering (reflection) from the hologram, and it is located symmetrically with respect to the transmitted plane wave.

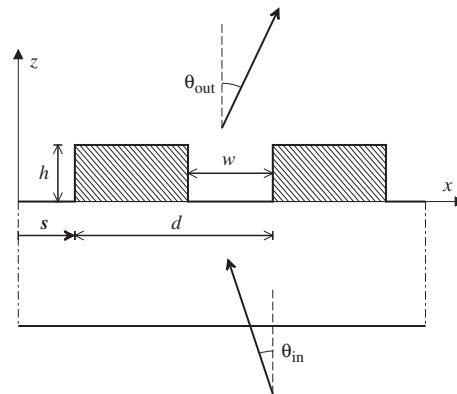


Figure 6. Grating geometry and parameters for local rigorous optimization. The period d is determined through the local period of the transmittance while the groove depth h and width w are to be optimized to obtain a proper transmission amplitude for the diffraction order from θ_{in} into θ_{out} . The entire grating is further displaced by the vector s in order to correct local phase deviations. For an amplitude hologram, the thickness h of the copper layer is constant.

computed at a distance of 3 m; the plane wave is directed into the direction of 33° with respect to the hologram normal.

3.2. Local rigorous optimization

The FDTD-based design is only applicable when the hologram pattern can be assumed infinitely wide. Such an approximation does not hold for all holograms, e.g., for those used in generating Bessel beams. Then, alternative methods must be used. The holograms can be designed locally, assuming that the complex transmittance $T(x, y)$ has an approximately constant spatial frequency in the vicinity of each location on the hologram. This allows one to optimize the local grating profile with the use of rigorous electromagnetic theory [17]. A drawback is that the overall operation of the hologram is

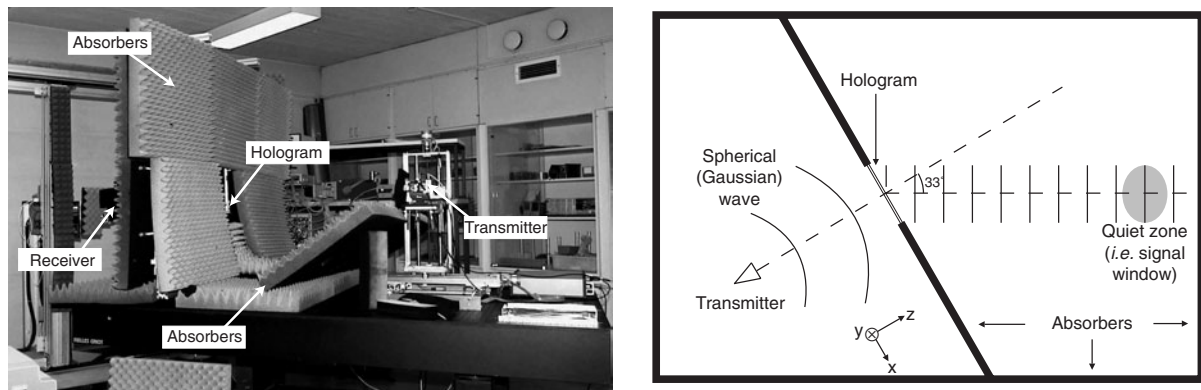


Figure 7. Hologram measurement set-up: the actual set-up in the Radio Laboratory at HUT (lhs) and a schematic illustration of an operating hologram (rhs).

not taken into account; edge diffraction, for instance, must be handled separately.

Radio holograms are often locally binary, i.e. the grating structure consists of a single groove of width w and depth h , see figure 6. The grating period d is the local spatial period of the transmittance; it is related to the incident angle θ_{in} and the diffraction angle θ_{out} by the grating equation $\sin \theta_m = \sin \theta_{in} + m\lambda/d$, where m is the diffraction order in question (in our case, $m = 1$ and $\theta_m = \theta_{out}$).

In the actual hologram design process, the required values of the amplitude modulation $a(x, y)$ and the phase modulation $\psi(x, y)$ (the absolute value and the phase of the transmittance) as well as the local grating period and the angle of incidence θ_{in} are determined at every point of the hologram. The optimal combination (w, h) is chosen to yield the desired transmittance. Local phase errors may then be corrected according to the detour-phase principle [18].

The unwanted diffraction effects can be reduced by choosing such a field distribution on the hologram that directly produces the desired field in the goal region (signal window). We refer to this algorithm as ‘back-propagation’; it consists of the following steps:

- (i) The beam profile, i.e. the amplitude and phase distribution of the electromagnetic field, is specified on the plane where the best fidelity is desired. The width of the beam has to be limited such that the error caused by the truncation of the transmitted field by the hologram aperture is minimized.
- (ii) The field is back-propagated to the hologram with the use of the angular spectrum representation [19]; the fast Fourier transform (FFT) algorithm can be efficiently utilized in the numerical implementation.
- (iii) The hologram structure is designed to convert the incident field into the output field calculated using back-propagation.

4. Measurement set-up

The required instrumentation for testing the radio holograms in the submillimetre-range of wavelengths includes a signal source with a feed, a receiver with a probe in a planar xy -scanner and a measurement controller. For measurements at the 310 GHz frequency, an AB Millimètre MVNA-8-350

network analyser and its extension parts ESA-1 and ESA-2 are used as the source and the receiver. A corrugated horn antenna for 310 GHz is used as the transmitting antenna and the receiving antenna is a pyramidal horn antenna. The receiver part is attached to a planar scanner controlled by a PC. For measurements of the beamsplitter (see section 5), the pyramidal horn antenna was replaced with an open-ended waveguide and the beamsplitter was illuminated with a plane wave generated using a binary amplitude hologram. The measurement arrangements are described in more detail in reference [20].

Absorbers are used for blocking the wave propagating straight from the transmitter to the receiver and also in order to minimize reflections, see figure 7. To avoid disturbances caused by waves propagating rectilinearly through the hologram aperture, the holograms are designed such that the transmitted beams propagate into an angle of 33° . Typical requirements for the CATR plane-wave field are a peak-to-peak amplitude ripple of less than 1 dB and a phase ripple less than 10° . The volume where the amplitude and phase ripples are sufficiently small is called the quiet zone. In the beamsplitter measurement, the beamsplitter was placed within a quiet zone of a CATR hologram and it was surrounded with absorbers.

5. Experimental results

Several holograms have been designed and fabricated for the CATR applications and also in order to produce more complicated beams, such as Bessel beams and vortices. The first plane-wave holograms were designed using the elementary binary quantization scheme with certain artificial tapering but, today, they are always optimized with the use of electromagnetic modelling. The first Bessel-beam and vortex holograms presented here were designed using an elementary scheme based on scalar diffraction theory [11]; the local optimization and the back-propagation method are, however, currently being implemented. The phase-type beamsplitter has been optimized using the rigorous theory of diffraction gratings [12, 21] and it has a sharp square aperture with no tapering.

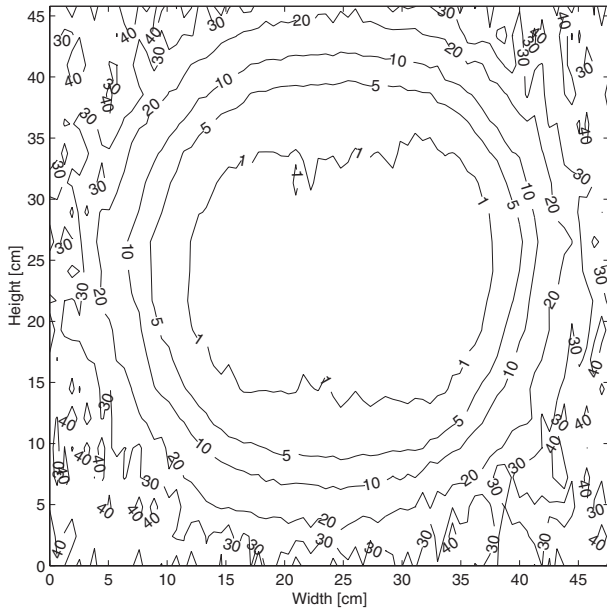


Figure 8. Measured quiet zone amplitude of the CATR hologram at 310 GHz. The contour plot is in the dB scale.

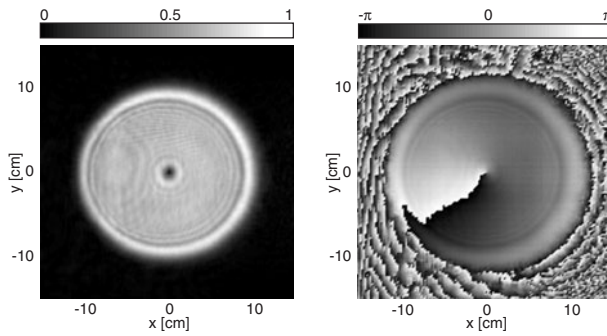


Figure 9. The amplitude (lhs) and phase (rhs) of the radio-wave vortex field measured at a distance of 16 cm from the hologram. For a singly charged vortex, the phase increases linearly by 2π for a path encircling the vortex axis.

5.1. Plane waves for CATR

A 60 cm hologram⁴ is designed and manufactured for 310 GHz to demonstrate the operation of the compact antenna test range at submillimetre wavelengths [5]. The goal is to achieve a flat amplitude and phase distribution in the quiet zone. Figure 8 shows the contour plot of the measured amplitude of the wavefront produced. The distance from the hologram to the measurement plane is 1.5 m. The peak-to-peak amplitude variation is within 1 dB in an area of about 25 cm \times 20 cm.

5.2. Electromagnetic vortices

Here we report the first results on an electromagnetic vortex at submillimetre-wave frequencies, analogous with optical vortices. The field is tapered to form a disc of diameter 20 cm where the amplitude of the vortex field is nearly constant. The phase of the vortex is designed to rotate around a loop

⁴ The manufactured hologram was later found to have a smaller diameter than the designed 60 cm, because the narrowest slots were not etched open in the lithographic manufacturing process used.

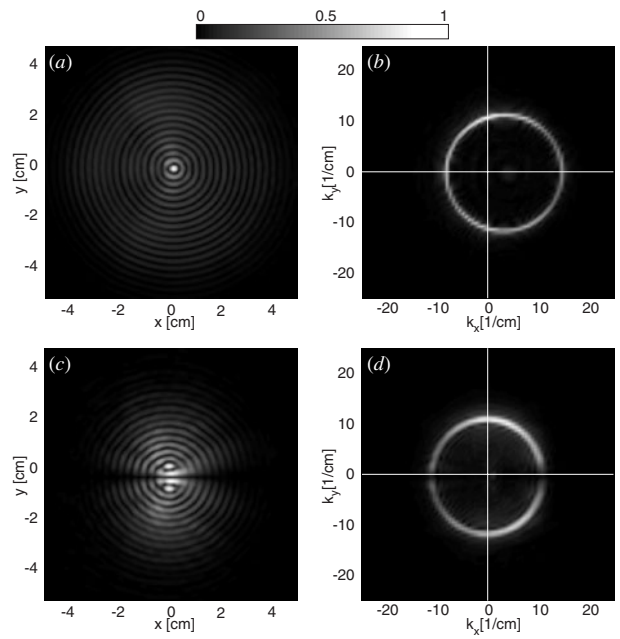


Figure 10. Bessel-beam measurement results. (a) Zeroth-order Bessel beam $J_0(\alpha r)$, and (b) its spatial Fourier transform (angular spectrum). This should be a circle of radius α , symmetrically situated around the origin. The displacement is caused by a linearly increasing phase along x and it is attributed to a 2.75° misalignment of the scanner plane. (c) Sine-type first-order Bessel beam $\sin(\varphi)J_1(\alpha r)$, and (d) its Fourier transform.

by 2π , hence resulting in the topological charge one. The field amplitude necessarily vanishes along the vortex axis so as to preserve continuity.

Figure 9 shows the field distribution and the phase of a singly charged vortex, measured near the hologram. In our measurements, diffraction rings are observed around the vortex, originating from the circular aperture. The intensity of the rings increases with distance from the hologram, in accordance with numerical simulations using an angular-spectrum representation of the vortex disc. Radial amplitude fluctuations also appear to cause azimuthal phase deviations (ideally, the phase would have a constant value along each radial direction).

5.3. Bessel beams

We have also fabricated and measured amplitude holograms that form radio-wave Bessel beams. Within a Bessel beam, the field energy is focused along the axis; thus, the hologram acts as an axicon lens [22]. Bessel beams are often called diffraction-free because the focal line of the beam (having a radius on the order of the wavelength) propagates without diffractive spreading. The central maximum is surrounded by several Bessel fringes of decreasing intensity for increasing distance from the beam axis. The field energy is directed onto the axis at the cone angle θ (also sometimes called the axicon angle); hence the Fourier transform of the field forms a ring with the radius $\alpha = (\omega/c) \sin \theta$.

Here we present two measured Bessel beams, namely the zeroth-order fundamental beam and the first-order beam whose azimuthal shape is given by the sinus function [23],

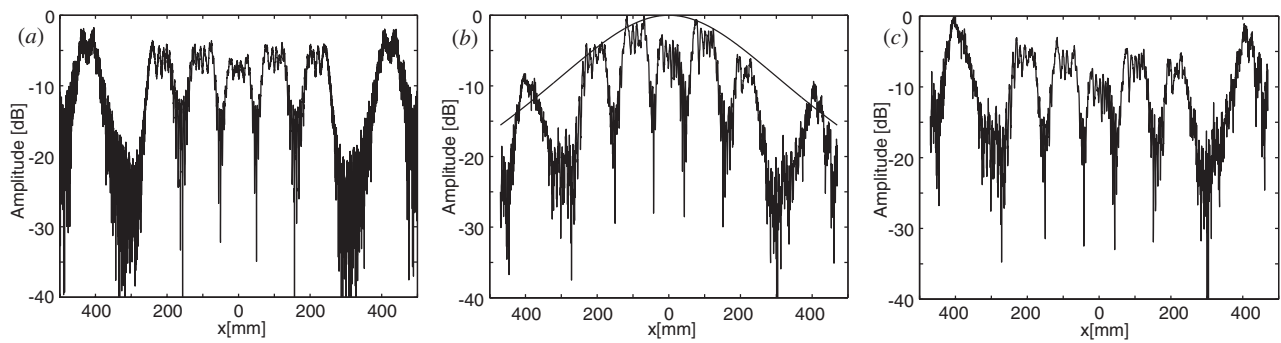


Figure 11. Phase-element beamsplitter results. (a) Calculated pattern at $z = 40$ cm. (b) Measured data and the theoretical directional pattern of the receiving waveguide. (c) Measured data corrected with the waveguide pattern. The shapes of the seven individual peaks show characteristic Fresnel diffraction with a Fresnel number of $N_F \approx 10$ [19].

see figure 10. The latter vanishes along the x axis where the phase has a discontinuity of π radians. We have used the cone angle $\theta = 10^\circ$; the ideal mathematical forms of these Bessel beams are $J_0(\alpha r)e^{i\beta z}$ and $\sin(\varphi)J_1(\alpha r)e^{i\beta z}$. The radial and axial wavenumbers are $\alpha = (\omega/c) \sin \theta \approx 1.13 \times 10^3 \text{ m}^{-1}$ and $\beta = (\omega/c) \cos \theta \approx 6.40 \times 10^3 \text{ m}^{-1}$, respectively.

5.4. Phase holograms

A beamsplitter phase hologram was produced and measured in order to test the material used and the fabrication method. The element was milled on a dielectric material substrate, Obomodulan[®], with the use of a computer-numerically-controlled milling machine. The size of the element is $80 \text{ mm} \times 80 \text{ mm} \times 10 \text{ mm}$ and 20 pairs of rectangular grooves were milled onto it. The widths of the grooves are 1.8 mm and 0.6 mm and the depth is 0.8 mm. The designed effect of the hologram is to redirect an incident plane wave into seven beams of equal intensity. Due to its square aperture, however, the diffracted beams unavoidably suffer from edge diffraction. For the expected pattern of the transmitted field, see figure 11(a).

Figure 11(b) shows the measured output and the radiation pattern of the receiving open-ended waveguide (as a function of x at a distance of 40 cm from the hologram). In figure 11(c), the measured data are corrected by dividing with the theoretical radiation pattern of the receiving waveguide. Qualitatively, the waveguide-corrected measurements are close to the expected pattern. However, the deviations may be due to several factors: (i) the attenuation of the radio field within the hologram was not taken into account in designing the hologram structure, (ii) the refractive index of the hologram substrate appears to vary⁵, and (iii) the computed waveguide-end radiation pattern was used, and it may differ from the actual pattern. Nonetheless, we consider the overall operation of the phase element satisfactory.

6. Conclusions

We have designed and fabricated both amplitude-type and phase-type holograms for submillimetre-wave frequencies. The primary application area of these techniques is in the

⁵ Measurements of the relative permittivity yielded values within $\epsilon_r = 2.2 \pm 0.1$, i.e. refractive index $n = 1.48 \pm 0.03$, depending on the piece of material measured and also on the location on it.

CATR for testing satellite antennas. We have also, for the first time, synthesized computer-generated holograms to produce nondiffracting Bessel beams and radio-wave vortex configurations at submillimetre-wave frequencies.

In addition to the binary quantization schemes applied in this work, several other coding schemes of phase and amplitude have also been suggested in the optical regime, utilizing subwavelength grating structures [3]. Such feature sizes are difficult to fabricate at optical wavelengths but they may in fact be readily realized in the radio-wave regime. Thus, the existence of a large variety of hologram techniques holds significant promise for radio-hologram research and radio-wave applications in the future.

Acknowledgments

Individual authors are grateful to the Foundation of Technology (Finland), the Foundation of the Finnish Society of Electronics Engineers, the Finnish Cultural Foundation, the Jenny and Antti Wihuri Foundation, the Foundation for Commercial and Technical Sciences and the Nokia Foundation for support. This research is also funded by the Academy of Finland through the Research Programme on Electronic Materials and Microsystems (EMMA), and by ESA ESTEC (ESTEC contract no 13096/98/NL/SB).

References

- [1] Lee W-H 1978 Computer-generated holograms: techniques and applications *Progress in Optics XVI* ed E Wolf (Amsterdam: Elsevier) pp 121–231
- [2] Wyrowski F and Bryngdahl O 1991 Digital holography as part of diffractive optics *Rep. Prog. Phys.* **54** 1481–571
- [3] Turunen J and Wyrowski F (ed) 1997 *Diffractive Optics for Industrial and Commercial Applications* (Berlin: Wiley)
- [4] Ala-Laurinaho J, Hirvonen T, Piironen P, Lehto A, Tuovinen J, Räsänen A V and Frisk U 2001 Measurement of the Odin telescope at 119 GHz with a hologram-type CATR *IEEE Trans. Antennas Propag.* **49** 1264–70
- [5] Säily J, Ala-Laurinaho J, Häkli J, Tuovinen J, Lehto A and Räsänen A V 2000 Test results of 310 GHz hologram compact antenna test range *Electron. Lett.* **36** 111–12
- [6] Durnin J, Miceli J J Jr and Eberly J H 1987 Diffraction-free beams *Phys. Rev. Lett.* **58** 1499–501
- [7] Turunen J, Vasara A and Friberg A T 1988 Holographic generation of diffraction-free beams *Appl. Opt.* **27** 3959–62

- [8] Salo J, Meltaus J, Noponen E, Westerholm J, Salomaa M M, Lönnqvist A, Säily J, Häkli J, Ala-Laurinaho J and Räisänen A V 2001 Millimetre-wave Bessel beams using computer holograms *Electron. Lett.* **37** 834–5
- [9] Monk S, Arlt J, Robertson D A, Courtial J and Padgett M J 1999 The generation of Bessel beams at millimetre-wave frequencies by use of an axicon *Opt. Commun.* **170** 213–15
- [10] Vasnetsov M and Staliunas K (ed) 1999 Optical vortices *Horizons in World Physics* vol 228 (New York: Nova Science Publishers)
- [11] Vasara A, Turunen J and Friberg A T 1989 Realization of general nondiffracting beams with computer-generated holograms *J. Opt. Soc. Am. A* **6** 1748–54
- [12] Petit R (ed) 1980 *Electromagnetic Theory of Gratings* (Berlin: Springer)
- [13] Yee K S 1966 Numerical solution of initial boundary value problems involving Maxwell's equations in isotropic media *IEEE Trans. Antennas Propag.* **14** 302–7
- [14] Hirvonen T, Ala-Laurinaho J P S, Tuovinen J and Räisänen A V 1997 A compact antenna test range based on a hologram *IEEE Trans. Antennas Propag.* **45** 1270–6
- [15] Ala-Laurinaho J, Sehm T, Säily J and Räisänen A V 2000 Cross-polarization performance of the hologram compact antenna test range *Microw. Opt. Technol. Lett.* **27** 225–9
- [16] Berenger J-P 1994 A perfectly matched layer for the absorption of electromagnetic waves *J. Comput. Phys.* **114** 185–200
- [17] Noponen E and Turunen J 1996 Complex-amplitude modulation by high-carrier-frequency diffractive elements *J. Opt. Soc. Am. A* **13** 1422–8
- [18] Lohmann A W and Paris D P 1967 Binary Fraunhofer holograms, generated by computer *Appl. Opt.* **6** 1739–48
- [19] Goodman J W 1996 *Introduction to Fourier Optics* 2nd edn (New York: McGraw-Hill)
- [20] Räisänen A V *et al* 2001 Computer generated holograms for mm- and submm-wave applications: CATR, Bessel beams and radiowave vortices *Proc. 9th Int. Conf. on Terahertz Electronics (Charlottesville, Virginia, Octo.)* at press
- [21] Noponen E, Vasara A, Turunen J, Miller J M and Taghizadeh M R 1992 Synthetic diffractive optics in the resonance domain *J. Opt. Soc. Am. A* **9** 1206–13
- [22] McLeod J H 1954 The axicon: a new type of optical element *J. Opt. Soc. Am. A* **44** 591–7
- [23] Salo J, Fagerholm J, Friberg A T and Salomaa M M 2000 Unified description of nondiffracting X and Y waves *Phys. Rev. E* **62** 4261–75